Modelling the Thyroid Geometry

Giulia Spaletta

Mathematics Department, Bologna University, Piazza Porta S.Donato 5, I–40127 Bologna, Italy.
spaletta@dm.unibo.it

Given a single bidimensional ultrasonogram or scintigraphic image, we consider the feasibility for a tridimensional reconstruction of a human gland or organ. In particular, the reconstruction of one lobe of the thyroid gland is considered. The output sought, besides the visualization of the organ in space, is the approximation of the functional and morphological volume of the organ; this value is also taken as the approximation of the vascularization volume.

Blood vessels in the human body have complex branching structures and recent studies indicate that they are likely to have a fractal element in their aggregation. In this work, we initiate a study of the possibility for recreating the geometry of the thyroid arteries. By employing an angiographic image, showing the entire profile of one thyroid lobe, we analyze the feasibility of identifying its arterial reticule. An image analysis approach is followed for studying the fractal nature of the thyroid arterial tree geometry. The aim is to understand whether it is practicable to model the lobe vascular framework, in such a way that it represents the correct anatomical network, on which to design an organ that maintains the morphological and physiological features of the thyroid gland.

We will discuss the features of *Mathematica* that are useful in modeling each phase of the problem considered: image data acquisition, analysis and visualization. *Mathematica* represents an ideal framework for the creation of prototypal procedures and the development of new algorithms, as it is now fast enough for 2D and 3D image analysis. The symbolic and numeric capabilities of *Mathematica* are exploited, together with its facilities for importing and rendering image data of various origin, as well as for data approximation. Image processing and graphical tools are also employed, for the shape analysis and reconstruction.

Keywords: *edge detection; data approximation; volume estimation; vascularization volume; fractal branching model.*

■ 1. Introduction

A single echographic, scintigraphic or angiographic image of one lobe of the thyroid gland is considered. The focus is on patients affected by a particular pathology of the thyroid, namely the *Plummer's nodule.* The ideas that will be pursued in this work, in the tridimensional treatment of the lobe, can be applied to other human glands and organs, as long as their morphology is similar to that of the thyroid.

Currently the volume of a thyroid is estimated as half the volume of a parallelepiped, using the measures of its three axes as provided by the echographer. Aside from the tridimensional visualization of the thyroid lobe, the scope is to provide a numerical approximation to the lobe volume that is more accurate than the current way of estimating it [Spaletta:2004].

Through the tridimensional information obtained, the aim is to perform both a functional and morphological analysis of lobes affected by the Plummer's nodule, to establish such a pathology with the least invasive and expensive examination.

There exists a relation between the occurrence of the Plummer's pathology and the vascularization of one lobe. It is thus important to identify its arterial reticule and to design a model for the thyroid arterial tree geometry. Our study, currently at an initial state, follows a fractal branching approach, to reproduce the lobe vascular framework. In doing so, the aim is to preserve the morphological and physiological features of the thyroid gland.

This paper is organized as follows. The medical problem is explained in § 2, in which details of the morphology and functions of the thyroid gland are given. The numerical model and solution method are described in § 3, containing an outline of the procedures for the data collection and approximation, as well as the volume evaluation and the tridimensional visualization techniques [Gray:1998], [Gonzalez:2002]; a numerical example is given in § 4. A variation of the proposed method, in the case of two input images, is outlined in § 5. The current research, on the fractal branching modelling of the thyroid arterial system, is briefly illustrated in § 6. Some conclusions are drawn in § 7.

■ 2. Thyroidal Morphology and Function

The thyroid is the biggest gland in the neck, situated in the anterior neck, below the skin and muscle layers. It takes the shape of a butterfly wrapped around the trachea, with the two wings represented by two lobes, left and right, connected in the middle by an isthmus.

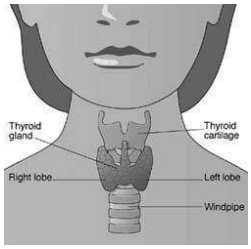

In an adult the gland generally weighs 20 grams, but this can vary noticeably. The dimensions also can vary; generally the three lobe diameters measure, in centimeters: 5—6 (height, in the vertical or coronal plane); 2—3 (width, in the horizontal or transverse or axial plane); 1—2 (depth, in the longitudinal or sagittal plane). By dividing the height in three uniform intervals, each lobe can be ideally divided into three parts, called *upper, central and lower thirds*.

The thyroid is an *endocrine* gland, producing internal hormonal secretions, in particular triiodothyronine (T3) and thyroxine (T4), that increase the cellular activity of nearly all body tissues. The thyroid function is thus to regulate the metabolism, that in turns affects many apparatus, like renal and respiratory apparata and the circulatory system; it also have an important effect on the growth and evolution of the human body.

□ Plummer's Nodule

Plummer's disease is a disorder in which a part of the thyroid tissue is functioning autonomously (toxic nodule) from the rest of the gland (*parenchyma*, normal tissue) and producing excess hormones. It is characterized by the presence of a single hyperfunctioning *hot* nodule within one lobe of a normal thyroid gland; the evolution of the nodule can lead to a progressive suppression of the remaining thyroid parenchyma.

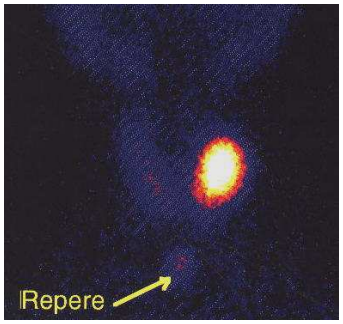

The clinical signs are hyperthyroidism and cardiovascular manifestations, such as tachycardia, atrial fibrillation, congestive heart failure. Weakness, muscle wasting, emotional lability are common. Eye symptoms usually do not occur, unlike for other thyroid diseases. The Plummer's pathology is generally benign. The progressive growth of the nodule, though, can cause airway or digestive tract obstruction, leading to dyspnea (shortness of breath), dysphagia (difficulty in swallowing), dysphonia (altered voice production), and may require emergent thyroid surgery.

□ Thyroid Arteries and Lobe Shapes

Blood is a circulating tissue, composed of a fluid (plasma) with suspended elements (red and white blood cells and platelets). Arterial blood is the means by which oxygen and nutrients are transported to tissues. Venous blood is the means by which carbon dioxide and metabolic by−products are transported for excretion. No blood flowing through a nodule is an indication that the tissue is not live (likely a cyst), suggesting a benign nodule.

For each lobe the are a *superior thyroid artery* (STA) and an *inferior thyroid artery* (ITA). The following figure shows how the STA and ITA supply the lobes of two thyroids, with *oval and conic lobes respectively.*

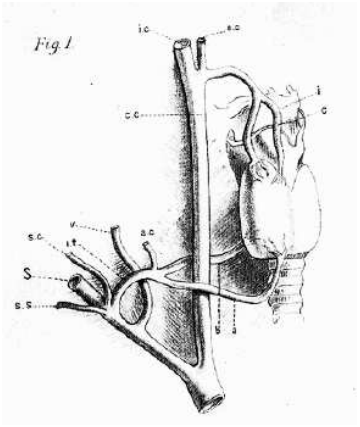

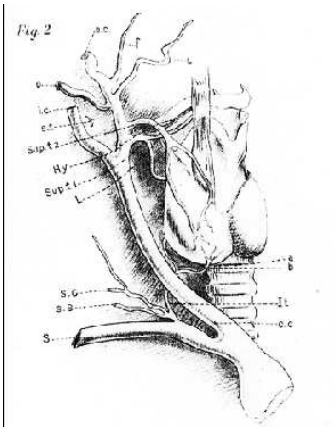

Based on shape, a classification of the lobe can be done: *oval* or ellipsoidal lobe, observed in one third of the population; *conic* or pear—shaped lobe, that occurs in two third of the population. In [Toni:2002a], [Toni:2002b] a relation is considered between the occurrence of the Plummer's pathology and the dominance of the STA or ITA in the vascularization of one lobe. In an oval shaped lobe it has been observed a STA dominance; in a conic shaped lobe it has been noted an ITA dominance.

The Plummer's nodule is highly vascularized and highly functioning. Its formation and survival are strictly depended on the vascularization of the parenchyma assaulted by this pathology. As a consequence, it is more likely that a nodule is a Plummer's one if it is in the upper third and if there is a STA dominance (oval lobe). Analogously, it is more likely that a nodule is a Plummer's nodule if it is in the lower third and if there is an ITA dominance (conic lobe).

A computation, from the data contained in a single ultrasonogram, of the vascularization volume is important to obtain therapeutic and pharmacological indications. It is also important to avoid further examination and possibly also avoid surgical extraction. Finally, it is important since it could be used to minimize the need for post—surgical examination.

In all the above, *hypothesis of uniformity* in the tissue and in the arterial distribution, extension and density are made. These assumptions can be reasonably made in the case of a thyroid lobe and nodule. They also apply to other organs or glands in the human body, such as liver, kidneys, lungs, suprarenal glands, hypophysis, ovaries, testicles, mammary glands, etc. The finding of this work thus can be extended to the study of the organs and glands mentioned.

■ 3. Numerical Model

The input data to our problem is represented by the scan of a bidimensional image of one thyroid lobe affected by the Plummer's pathology. A scintigraphic image is considered, but the same ideas can be applied to an ultrasound image. Colors are rendered as gray levels by means of the formula: *gray = 0.299 red + 0.587 green + 0.114 blue*.

The output sought, besides the visualization of the lobe in space, is (under spacial uniformity assumptions) the approximation of the functional/morphological volume of the lobe thirds and of the nodule, as well as the approximation of the center of gravity of the lobe and of the nodule (these two centers are used to determine the incidence of the nodule inside each of the thirds).

The lobe is classified according to its shape, established by a simple observation: in an **oval** lobe, the volume proportion between the upper third and the entire lobe is equivalent to the volume proportion between the lower third and the lobe; in a **conic**

lobe, the volume proportion between the upper third and the entire lobe is smaller than the volume proportion between the lower third and the lobe.

By utilizing the output data, an analysis of the statistical correlation between the lobe shape and the relative position of the centers of gravity is performed. A relation is obtained between the lobe shape and the incidence of the Plummer's pathology (within a particular third of the lobe). Such results represent the medical motivation for this work.

From the numerical point of view of computational mathematics, the motivation for this project is a feasibility study of reconstructing a tridimensional volume from data contained in one bidimensional image. The approximated volume has to fulfill criteria of accuracy, while the implementation of the reconstruction method must be robust and efficient in terms of memory requirements, computational time and cost.

□ Algorithm Outline

The ingredients for the algorithm are as follows.
▫ The gray level bidimensional image is stored as a matrix, in which an **edge detection** method (plus some refining technique) is applied in order to determine the border of the thyroid lobe (or nodule).
▫ The border points are collected into two separate sets, in such a way that each set can be **approximated by a function**; in other words, the lobe edge is split into two *silhouettes*, say **s1** and **s2**, *of known analytic form* (two spline functions, for example).
▫ A parametrization in space is applied in order for **s1** to rotate and be **smoothly deformed** into **s2**. In this way a tridimensional object is obtained, with known analytic expression, that can therefore be **integrated** to obtain the volume value.
▫ The center of gravity of the lobe (or nodule) can also be easily computed from the collected data.
The following subsections describe the reconstruction steps in more detail.
Here are the preliminaries in *Mathematica*, that are required for the algorithm implementation.

```
Off[General::spell1];
<< Graphics`Graphics`
<< LinearAlgebra`MatrixManipulation`
<< DiscreteMath`ComputationalGeometry`
<< Statistics`DescriptiveStatistics`
<< Graphics`ParametricPlot3D`
<< Graphics`Graphics3D`
```

□ Edge Detection and Data Collection

The built–in **Import** routine is used to acquire the scintigraphy data, in the correct format, and convert it to a *Mathematica* expression.

```
filename = "tiroide7j.jpg";
img = Import[filename, "JPEG"];
```

Given a matrix, whose elements are RGB vectors, **getChannels** yields three matrices, one for each color component; **grayCut** defines the transformation from colors to gray scale; **myShow** renders the data as a grey scale matrix.

```
{red, green, blue} = getChannels[img[[1, 1]]];
cutArea = {{411, 620}, {165, 300}};
grayCut = 0.299 * Take[red, cutArea[[1]], cutArea[[2]]] +
   0.587 * Take[green, cutArea[[1]], cutArea[[2]]] +
   0.114 * Take[blue, cutArea[[1]], cutArea[[2]]];
myShow[grayCut];
```

Thyroid3D is the name of the prototypal package that implements the algorithm and that needs to be loaded.

```
<< Thyroid3D'
```

The inputs are as follows.
▫ The *grey scale image* (of one thyroid lobe); two integers in a scaled range [0, 100], used as a probability percentage, to determine the image regions containing the lobe and nodule baricenters, respectively.
▫ Two *thresholds* for pre− and post−processing the current image, before and after edge detection, respectively; the thresholds can be initially set equal to the pixel average value, but adjustment might be necessary, using information from the gradient image histogram.
▫ A parameter *alpha* used when determining the two separate sets of border data (for penalizing horizontal versus vertical discrepancies).
▫ The approximant spline *degree*; the *number* of approximation points; the values of the spline *derivative values* at left and right interval ends.
▫ A *boolean* option for visualizing intermediate images.

```
percentBaricenterLobe = 35;
percentBaricenterNodule = 85;
thresholdBeforeEdgeDetection = 70;
thresholdMagnitudeGradient = 220 ;
alpha = 10;
degree = 3;
numberApproximationPoints = 30;
derivativeLeft = 10;
derivativeRight = -4;

{s1, s2, maxHeight, baricenterLobe, baricenterNodule} =
  Thyroid3D[grayCut,
   percentBaricenterLobe, percentBaricenterNodule,
   thresholdBeforeEdgeDetection, thresholdMagnitudeGradient,
   alpha, degree, numberApproximationPoints,
   derivativeLeft, derivativeRight, False];
```

The outputs are: the two *approximants*; the lobe *height*; the positions of the lobe and nodule *baricenters*, respectively.

The following figure collects the intermediate images, from left to right:
▫ the grey scale image stored as a matrix;
▫ a black/white image obtained from the grey scale using the first threshold;
▫ a blurred image, obtained via convolution of the b/w image with a filter matrix, so that the less sharp parts of the border will be ignored by edge detection;
▫ the image yielded by edge detection;
▫ the image obtained after further border refining via the second threshold.

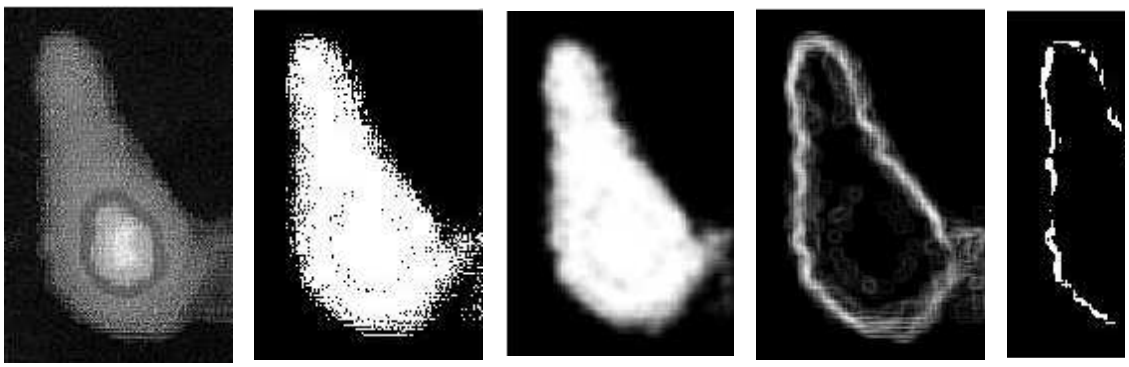

The following figure (from left to right) illustrates how the edge refined matrix is processed to determine a *dotted border*. The current matrix entries are 0 (*off*) or 1 (*on*). A horizontal row scan sets a pixel value to 1 only if there is a step from an *off* pixel to an *on* pixel, otherwise it sets it to 0. The same scan is repeated vertically, column by column. The resulting structure is a sparse matrix having a few unitary entries: the coordinates of pixels of value 1, representing the border points, can then be stored in an array and plotted via **ListPlot**.

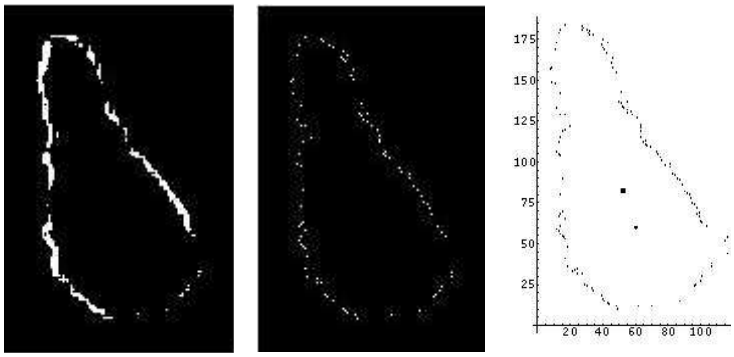

Note that an edge detection procedure is also available in the *Mathematica* third party package **Digital Image Processing**. Alternative edge detection strategies can be found in the literature [Marshall:2003], [Sonka:2003].

□ Data Approximation

Let **(xi, yi)** denote the lobe border data. These are subdivided into two sets w.r.t. a vertical axis **S** of symmetry, in such a way that points to the left of **S** define a function **f1** and points to the right of ***S*** define a function **f2**, with **f1** and **f2** defined on a communal domain of the independent variable **u**. The axis **S** is determined with the rotation procedure outlined below:

▫ minimum η**x** and maximum μ**x** values of the *xi* are computed, together with analogous values η***y*** , μ***y*** in the **yi**;
▫ a rotation angle is defined as θ **= ArcTan[(**μ**y − **η**y)/(**μ**x − **η**x)];**
▫ all data points are rotated according to θ.
The procedure is repeated until μ**y = **η**y**, that is θ **= 0**, or for a maximum number of iterations. Some adjusting might be necessary, to take into account the occurrence of multiple data with η**x = **μ**x** and/or η**y = **μ**y**. Three iterations are generally sufficient to obtain $\theta \approx 0$ in this type of problem.

The first two images below (from left to right) illustrate the lobe data and the rotation, as well as lobe and nodule baricenters. The last two images show data separated in such a way that they can represent samples of two functions. Again simple calls to **ListPlot** are sufficient for visualization.

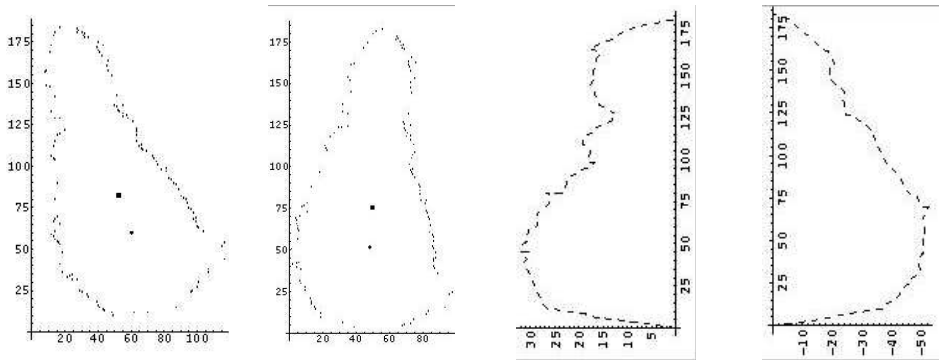

Points to the left of the axis **S** are denoted **(u, f1(u))**, those to the right of **S** are **(u, f2(u))**. Approximants **s1** and **s2** to the functions **f1** and **f2** can be recovered by data approximation. *Least squares* approximation is used here, with polynomials or splines, constrained to use derivative information, for smoothness, at the end points of the range [0, **maxHeight**] of the variable **u** [Dierck:1995].

Note that the standard package **NumericalMath** makes available various numerical data approximants. **PolynomialFit** computes a least squares polynomial approximant of a desiderated degree, choosing a more appropriate base than simple powers of a variable; it returns a pure function, that can be evaluated in a numerically stable way. **SplineFit** works in a similar way, yielding a spline approximant. A least squares trigonometric approximant could also be considered, using **TrigFit**.

The first two images below (from left to right) illustrate the rotated lobe data, visualized via the **PlotJoined** option of **ListPlot**. The last image is the **Plot** of the two approximants **s1** and **s2**.

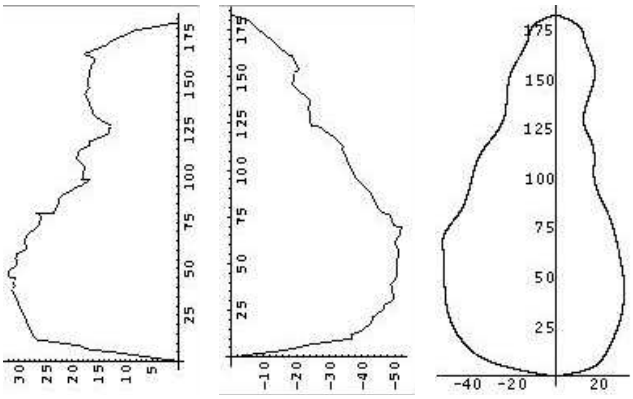

□ Parametrization

A parametrization in space is applied in order for **s1** to *rotate* and be *smoothly deformed* into **s2**. Images in the following figure illustrate the idea by employing two synthetic silhouettes. A pure rotation in space w.r.t. the axis **S** would not be sufficient to obtain a closed tridimensional object (see, below, the image to the far right).

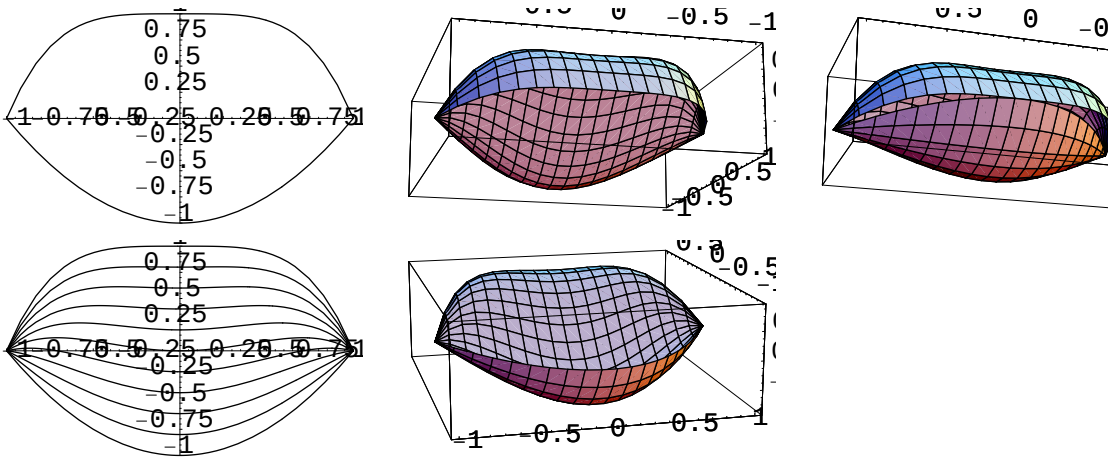

Among the different choices of parametrization, we considered for example

$$(u,\ \rho) \mapsto (S(u,\rho)\cos(\rho),\ S(u,\rho)\sin(\rho),\ u)$$

$$S(u,\rho) := s_1(u)\ \frac{1+\cos(\rho)}{2} + s_2(u)\ \frac{1-\cos(\rho)}{2}$$

As the angle ρ ranges from **0** to π, a rotational smooth movement is performed, in space, from **s1** ($\rho = 0$) to **s2** ($\rho = \pi$).

□ Volume

With the correct parametrization a tridimensional object is constructed and can be visualized with **ParametricPlot3D**.

```
S[u_, rho_] :=
  s1[z] * (1 + Cos[rho]) / 2 + s2[z] * (1 - (1 + Cos[rho]) / 2);
ParametricPlot3D[{S[u, rho] Cos[rho], S[u, rho] Sin[rho], u},
  {u, 0, maxHeightF}, {rho, 0, 2 Pi}, PlotPoints → {100, 100},
  ImageSize → 5 * 72, Axes → False, Shading → False];
```

It is also possible to highlight the three lobe thirds in colors.

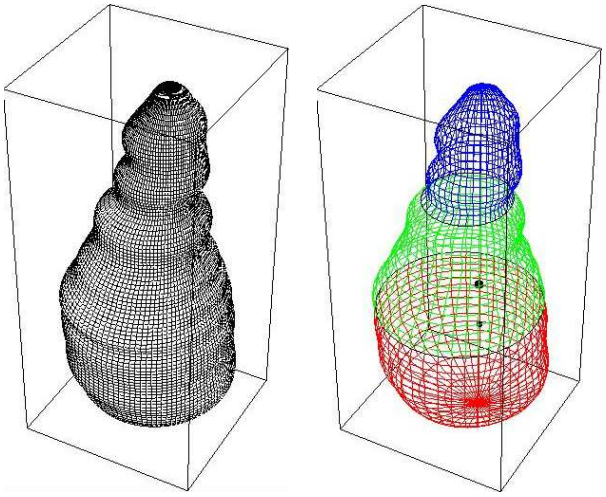

As the analytic expression of the tridimensional object is known, its volume can be computed by numerical integration, with **NIntegrate**. The inner integration range is [A,

B] = [0, **maxHeight**] to obtain the lobe volume. The volumes of each of the lobe thirds can be computed by varying the integration range: [0, B/3] for the (red) lower third; [B/3, 2 B/3] for the (green) middle third; [2 B/3, B] for the (blue) upper third.

$$V = \frac{1}{2}\int_0^{2\pi}\int_A^B \left(S(u,\rho)^2\cos(\rho)^2 + S(u,\rho)^2\sin(\rho)^2\right) du\, d\rho$$

```
VolumeLobe =
 NIntegrate[S[u, rho]^2, {z, A, B}, {beta, 0, 2 Pi}] / 2 /.
  {A → 0, B -> maxHeight}
```

The procedure followed to reconstruct the lobe volume can be repeated for the nodule. From the data collected, both the lobe and nodule baricenters are computed, implementing the mathematical definition of gravity center.

■ 4. Numerical Test

Computations are performed on a 2.13 GHz Pentium 4M laptop, with 1 GB of RAM, running Red Hat Linux Fedora Core 4 and *Mathematica* version 5.2.0.

The scintigraphic image of the thyroid of a woman (aged 37) is the input. Provided by an accompanying echography, the nodule measures are in centimeters 30.8 (height), 18.7 (width), 17.1 (depth). The volume estimated by the radiologist is (30.8×18.7×17.1)/2 = 4.924 cm^3 . The following figure shows the tridimensional reconstruction of the nodule, with volume value 5.379, as computed by our methods. The reconstruction (elapsed) time is less than twelve seconds.

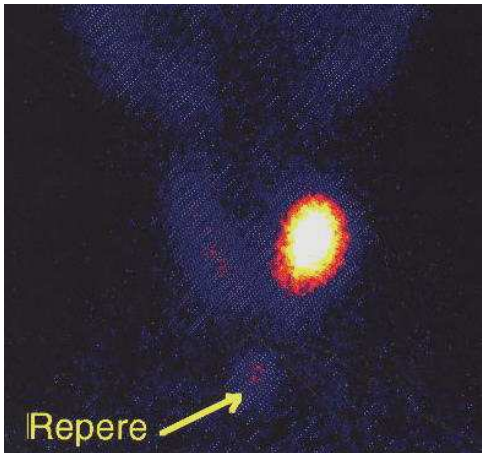

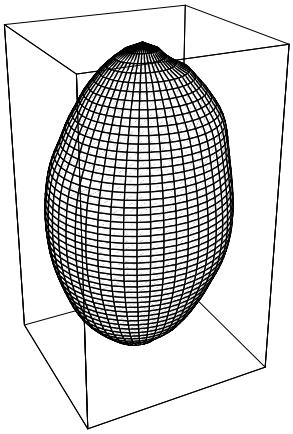

■ 5. Two Image Input

Echographic examination always provides two bidimensional images of the organ, projected on two planes that can be considered orthogonal to each other. If this is the case, it is worth including the information provided by both *vertical and horizontal reference images*, in the tridimensional reconstruction.

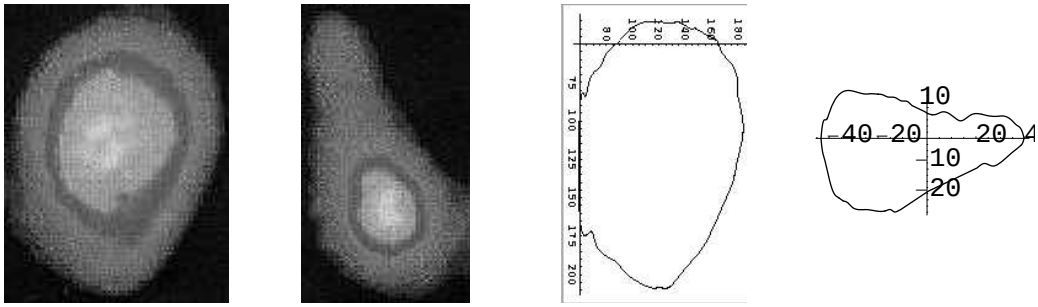

The procedure for edge detection and data approximation is used on both images, yielding a pair of approximants **s1** and **s2** in the vertical plane, as well as a pair of approximants **r1** and **r2** in the horizontal plane. Approximants **s1** and **s2** are treated as seen in the case of a single reference image. Approximants **r1** and **r2** are used to estimate the correct depth of each point on the surface that is being formed in space. If we intersect the reconstructed tridimensional object with planes parallel to the original horizontal one we therefore obtain horizontal sections with the same shape (though scaled and translated) as the initial horizontal reference image.

In the case of two reference images, the spatial parametrization is:

$$(u,\ \rho) \mapsto (S_x\ (u,\ \rho),\ S_y\ (u,\ \rho),\ u)$$

$$S_x\ (u,\ \rho) :=$$

$$\left\{s_1\ (u)\ \frac{1+\cos\ (\rho)}{2} + s_2\ (u)\ \left(1 - \frac{1+\cos\ (\rho)}{2}\right)\right\}\ \cos\ (\rho)$$

$$S_y\ (u,\ \rho) :=$$

$$\left\{s_1\ (u)\ \frac{1+\cos\ (\rho)}{2} + s_2\ (u)\ \left(1 - \frac{1+\cos\ (\rho)}{2}\right)\right\}\ F\ (u,\ \rho)$$

$$F\ (u,\ \rho) := \{\ k\ (\text{maxWidth})\ r_1\ (u)\ \text{if}\ \rho < \Pi;$$
$$k\ (\text{maxWidth})\ r_2\ (u)\ \text{if}\ \rho > \Pi\ \}$$

The interval [0, **maxWidth]** is the domain of the approximants **r1** and **r2**. The parameter **k** is computed as the maximum width allowed at a certain height, as it is used for scaling and translating the horizontal sections.

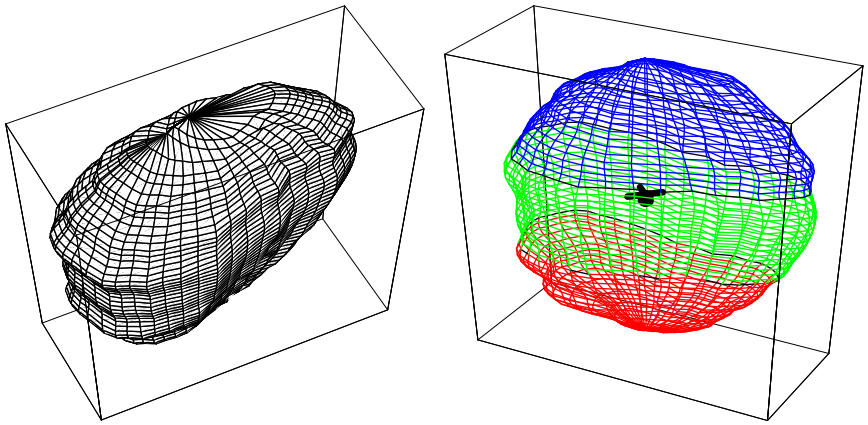

■ 6. Fractal Model

In this work, a feasibility study is initiated for the possibility of recreating the thyroidal artery geometry. By analyzing angiographic images, showing the entire contour of one lobe, we are trying to establish a fractal nature for the thyroid arterial network and to model its vascular structure accordingly. This has to be done so to allow for the correct design of a synthetic scaffold, to be potentially employed in the thyroid tissue engineering.

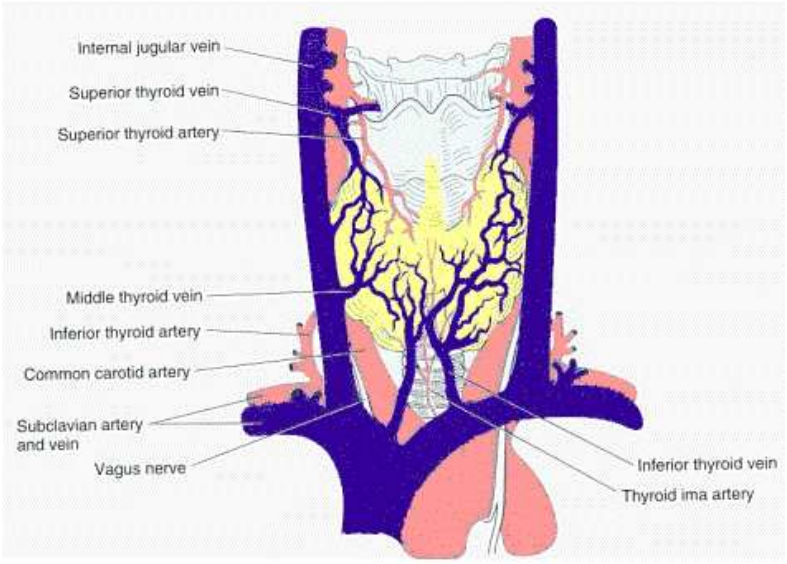

The branching geometry of arterial blood vessels in the human body suggests that they may have a fractal structure [Barnsley:1988]. They do not scale over an infinite range, as pure mathematical fractals do, but it is possible that a fractal element could be detected between the scales of the main supplying artery and the arterioles [Falconer:1990], [Kaandorp:1994].

The application of fractal rules to simulate biological systems has been proven to reflect the texture, within an organ, and the regional flow distribution. Many physical phenomena are governed by only one or two fractal rules.

Growth by branching is a central algorithm in the development of most cells and organs. The reason for this common behavior among tissues is the common need to obtain nutrients and to remove waste. Like trees, the ratios of branch diameters and length tend to be constant.

There are relations that can be exploited to define a regular fractal tree. Let **l1** be the length of the aorta and **lc** the length of each arteriole. Assume that the current branch is **s** times shorter than the previous branch. After **n** recursions:

$$lc = s^n \; l1$$

and the total length of the arterioles is given by:

$$ltot = 2^n \; lc$$

Therefore if estimates of **l1**, **lc** and **ltot** are available, it is possible to compute the recursion depth **n**, as well as **s** which represents the *similarity dimension* of the regular

fractal. One way to characterize a fractal, in fact, is through the definition of its (non necessarily integer) dimension.

Due to its recursive nature, one way to fractal generation is via iterated functions, using repeated applications of translation, rotation and scaling (Iterated Function System).

A simple way to iterate functions with *Mathematica* is to use **Nest** or **NestList.** A tree in two dimensions can be described by a few parameters: θ := angle between branches; **s** := scale factor; **n** := depth. A tree in three dimensions can be created by adding a further parameter: **m** := number of branches from previous branch [Cabrera:2000].

```
<< Geometry`Rotations`

NewBranch[θ_, s_][Branch[r1_List, r0_List]] :=
  Module[{r}, r = r1 - r0;
   {Branch[r1 + s RotationMatrix2D[θ].r, r1],
    Branch[r1 + s RotationMatrix2D[-θ].r, r1]}];

NewBranch[θ_, s_][w_List] := Map[NewBranch[θ, s], w];

Tree2D[θ_, s_, r_List, n_] :=
  NestList[NewBranch[θ, s], Branch[r, {0, 0}], n] /.
   Branch[x__] :> Line[{x}];
```

Setting `θ = π / 6, s = 8 / 10, r = {0, 1}, n = 6,` and calling **Show** to render **Graphics[Tree2D[*θ*,s, r,n]]** gives the following image:

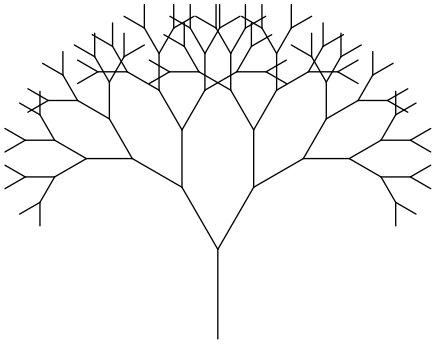

We can store the edge points, at the arterioles level, which define the border of the organ under consideration.

```
ntake = 2^n;
Take[Flatten[Tree2D[θ, s, r, n]], -ntake];
data = Flatten[Level[%, {2}], 1] // Union;
ListPlot[data,
  PlotStyle → PointSize[0.02], AspectRatio -> Automatic];
```

From the border data, it is possible to obtain an estimate of the tridimensional volume, with the procedure described in § 3.

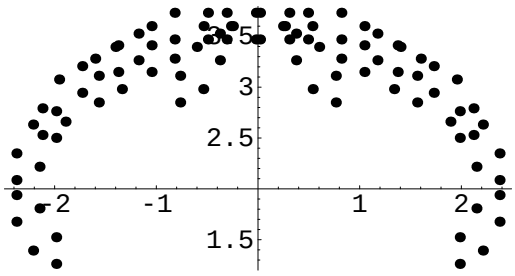

To directly build a tridimensional fractal blood network, it is necessary to impose a few constraints:

- place the current branch so that it avoids previous branches;
- prevent the current branch from going beyond the tissue limits.

Fractal branching models for coronary, pulmonary, renal arterial trees, as well as for the retina blood vessels, have been studied in the literature [Bassingthwaighte:1998], [Cross:1998]. For these vascular systems, optimal ratios of diameters, branching angles, and so on, have been computed. From such optimal measures, topologically appropriate reconstructions of the vascular tree can be built. The aim is to construct, from such data, a mathematical model that maintains the physiological features of the real tree, at least in a statistical sense.

A crucial part of our current project is the determination of optimal measures for these parameters for the thyroid gland.

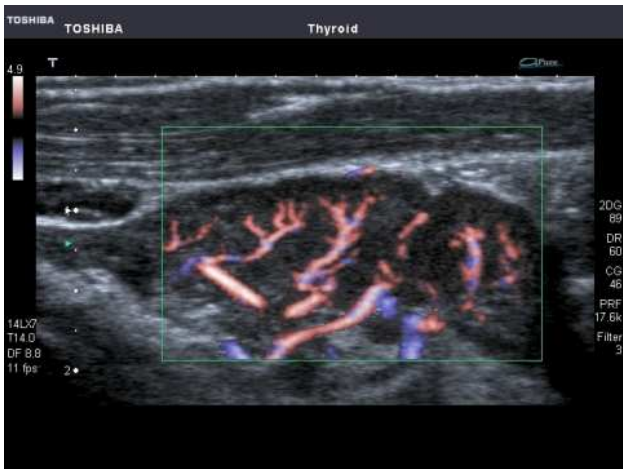

Image analysis represents a useful tool for the measurement of *fractal dimension* [Eins:1998]. Digital image analysis is a means of obtaining quantitative information (i.e. numerical data) from an image. Computer vision methods need a highly mathematical approach, in which differential geometry, partial differential equations, statistics, linear algebra, an so on, play a crucial role. In the current version of *Mathematica,* fast prototyping and design of new algorithms has become extremely efficient.

Tissue Engineering

Tissue loss represent a crisis in health care. Further to xenotransplantation, other therapeutic approaches are currently being pursued, such as the development of mechanical devices, for the replacement of organ function, and the rapidly emerging field of tissue engineering.

An approach to constructing replacement organs is to seed and expand autologous cells on microporous polymer constructs, engineered to replicate the structure and function of the target organ. This approach is constrained by the inability to generate complex tissues, due to oxygen transport limitations within the growing tissue. Nature solves this diffusion problem through the construction of a vast network of blood vessels, that permeate the organ at size scales ranging from 1 cm down to 10 μm. In developing vascularized structures, there are two main barriers:

- insufficient dimensional resolution (300 μm) in existing polymer processing methods;
- lack of suitable models for the design of the microcirculation.

There exists a substantial literature detailing the morphometry of blood vessel networks of the heart and liver. Fluid dynamics models produce the vascular networks for tissue engineered molds, with the aim of reproducing both the structural and the dynamic

properties of the vasculature. Fractal computation is used, as it accounts for the blood ability to flow or be deformed. The fractal approach attempts to emulate the adaptation and remodeling of microvascular structure, allowing for dynamic evolution of the design of the microvascular network [Peitgen:1992], [Rashevsky:1954].

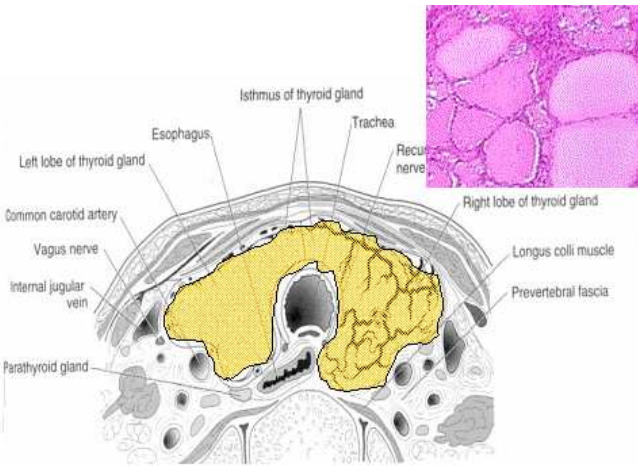

Our focus is on the structure of both the STA and ITA in a thyroid lobe. The ultimate aim is to establish a model for the design and construction of a polymer scaffold for organ replacement. For this ambitious aim, it is essential that the anatomical framework is represented correctly, so to maintain the morphological and physiological features of the thyroid gland.

■ 7. Conclusion and Future Work

The robustness of the method presented in this paper is essentially dependent upon the polynomial or spline approximation. The computational cost also coincides mainly with that of data approximation. Concerning the memory requirements, three matrices are needed, all of the same size: the first matrix stores the reference image values; two more matrices are needed to perform the edge detection procedure. The method application to a 256 x 128 image requires just a few seconds of elapsed time.

A tridimensional model of the thyroid, as well as of other organs or glands satisfying the assumption of spatial uniformity, is currently being investigated, which is essential to test the accuracy of the reconstruction.

A comparison with other techniques of reconstruction is also currently being carried out; the focus is in particular on methods that require only one (or two) reference images, such as the method described in [Falcone:1997].

The ease of use of the current routine is acceptable from the point of view of a numerical scientist, while an interface is still needed to make the software more accessible to medical researchers.

Our current research priority, however, is the development of a fractal branching approach to the modelling of the thyroid arterial system.

The resources available in *Mathematica* have been fundamental in developing the prototype algorithm implemented thus far. As well as the built−in resources, there are a variety of additional packages (such as fractal generation and edge detection) some of which available through *MathSource*, that ease the study of each phase of the problem considered. Symbolic and numeric capabilities of *Mathematica* are exploited, as well as

its facilities for image data manipulation. Performance, in terms of execution time and memory usage, allows for the efficient treatment of both planar or spatial objects.

■ Acknowledgments

This work stems from a cooperation with Roberto Toni, Anatomy Department at Bologna and Parma Universities, to which I am indebted. I am also grateful to Mark Sofroniou for useful discussions and help on various aspects involved in this project.

■ References

[Barnsley:1988] Barnsley MF, "Fractals everywhere", Academic Press, 1988.

[Bassingthwaighte:1998] Bassingthwaighte JB, Beard DA, King RB, ''Fractal regional myocardial blood flows: the anatomical basis'', in Fractals in Biology and Medicine, vol. II, edited by Losa G, Merlini D, Weibel E, Nonnenmacher T, Birkhauser, 1998, 114–127.

[Cabrera:2000] Cabrera Renan, ''Fractal Samples'', *MathSource,* 2000.

[Cross:1998] Cross SS, "Fractal geometry of the human renal arterial tree in development, health and disease", in Fractals in Biology and Medicine, vol. II, edited by Losa G, Merlini D, Weibel E, Nonnenmacher T, Birkhauser, 1998, 294–313.

[Dierck:1995], Dierckx P, ''Curve and Surface Fitting with Splines'', Oxford University Press, 1995.

[Eins:1998] Eins S, "Special approaches of image analysis for the measurement of fractal dimension", in Fractals in Biology and Medicine, vol. II, edited by Losa G, Merlini D, Weibel E, Nonnenmacher T, Birkhauser, 1998, 294––313.

[Falconer:1990] Falconer K, "Fractal geometry : mathematical foundations and applications", John Wiley, 1990.

[Falcone:1997] Falcone M, Sagona M, ''An Algorithm for the Global Solution of the Shape from Shading Model'', ICIAP, vol. 1 (1997) 596––603.

[Gonzalez:2002] Gonzalez RC, Woods RE, ''Digital Image Processing'', Prentice Hall, 2002.

[Gray:1998] Gray A, ''Modern differential geometry of curves and surfaces with *Mathematica*'', CRC Press, 1998.

[Kaandorp:1994] Kaandorp JA, "Fractal modelling : growth and form in biology", Springer, 1994.

[Marshall:2003] Marshall AD, ''Vision System'', Computer Science Dep., Cardiff University, www.cs.cf.ac.uk/Dave/Vision/

[Peitgen:1992] Peitgen H, Jurgens H, Saupe D, "Chaos and fractals : new frontiers of science", Springer, 1992.

[Rashevsky:1954] Rashevsky N, ''Topology and Life: in search of general mathematical principles in biology and sociology'', Bulletin of Mathematical Biophysics, vol. 16 (1954) 317––348.

[Sonka:2003] Sonka M, ''Digital Image Processing'', Engineering College, Iowa Univ., www.icaen.uiowa.edu/~dip/LECTURE/Segmentation3.html

[Spaletta:2004] Spaletta G, ''Approximation of a 3D Volume from one 2D Image. A Medical Application'', Atti della Accademia delle Scienze, Universita' di Bologna, serie I, vol. II (2004) 49−−65.

[Toni:2002a] Spaletta G, Toni R, et al, "A Study of the Arterial Dominance in the Human Thyroid Gland in relation to the Geometry of the Thyroid Lobe", Journal of Endocrinological Investigation, vol. 25, n. 6 (2002) 44.

[Toni:2002b] Spaletta G, Toni R, et al, " The Geometry of the Thyroid Lobe is a Determinant for Arterial and Nervous Dominance in the Thyroid Gland", Italian Journal of Anatomy and Embriology, vol. 107, n. 3/1 (2002) 269.

[Weisstein] Weisstein E, ''World of Mathematics'', Wolfram Research Editions, mathworld.wolfram.com/